Textile structured metacomposites with tailorable negative permittivity under X and Ku band

Qian Jiang [a, b], Chunjie Xiang [a, b], Yang Luo [c], Liwei Wu [a, b, **], Qian Zhang [a, b], Shilu Zhao [c], Faxiang Qin [c, ***], Jia-Horng Lin [a, b, d, *]

[a] Tianjin and Ministry of Education Key Laboratory for Advanced Textile Composite Materials, Tianjin Polytechnic University, Tianjin, 300387, China
[b] Innovation Platform of Intelligent and Energy-Saving Textiles, School of Textiles, Tianjin Polytechnic University, Tianjin, 300387, China
[c] Institute for Composites Science Innovation (InCSI), School of Materials Science and Engineering, Zhejiang University, Hangzhou, 310027, China
[d] Laboratory of Fiber Application and Manufacturing, Department of Fiber and Composite Materials, Feng Chia University, Taichung, 40724, Taiwan

HIGHLIGHTS

- Metamaterial units are built by interweaving ferromagnetic microwires into textile preform.
- Single negative characteristic is achieved by controlling curvature and arrangement of microwires.
- Curvature and arrangement of microwires affect electromagnetic response and microwave propagation.
- Electric loss is the main loss for metacomposites under X and Ku bands.

GRAPHICAL ABSTRACT
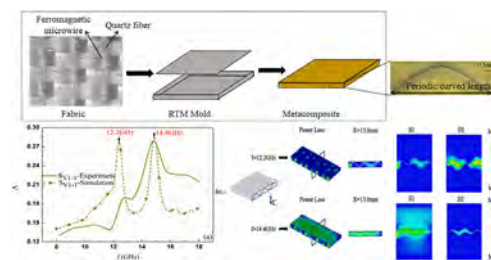
ARTICLE INFO

ABSTRACT

The metacomposites with tailorable negative permittivity including periodic interweaving ferromagnetic mircowires were fabricated by weaving and resin transfer molding methods. By manipulating the alignment direction, periodic curved length, spacing between ferromagnetic microwires for adjusting complex permittivity and permeability, the electromagnetic wave propagation of as-prepared metacomposites under X and Ku bands were evaluated and investigated by experiment and simulation. For metacomposites composed of vertically arranged microwires, for both 1 mm and 0.5 mm spacing, the permittivity turned to negative in certain frequency bands. The simultaneous existence of short periodic curved length and spacing benefits the broadening of frequency band under which metacomposites exhibits single-negative behavior. Significant transmission windows are observed due to negative permittivity occurring at plasma frequency. The simulation results show major loss for the textile

* Corresponding author. Tianjin and Ministry of Education Key Laboratory for Advanced Textile Composite Materials, Tianjin Polytechnic University, Tianjin, 300387, China.
** Corresponding author. Tianjin and Ministry of Education Key Laboratory for Advanced Textile Composite Materials, Tianjin Polytechnic University, Tianjin, 300387, China.
*** Corresponding author.Institute for Composites Science Innovation (InCSI), School of Materials Science and Engineering, Zhejiang University, Hangzhou, 310027, China
E-mail addresses: wuliwei@tjpu.edu.cn (L. Wu), faxiangqin@zju.edu.cn (F. Qin), jhlin@fcu.edu.tw (J.-H. Lin).

structured metacomposites under X and Ku bands derives from electric loss, and small periodic curved length tends to form uniform power loss distribution.

1. Introduction

A metamaterial, also named as left-handed material or double negative material, is defined as an artificially engineered material that gains its properties from its structure rather than its constituents [1]. The artificially periodic units in metamaterial give rise to negative refraction and reverse Doppler effect, thus leading to diverse applications in the fields of radome covers, perfect lens, and nondestructive damage monitoring [2–5]. Due largely to the complicated manufacture and huge dissipation, the development and application of metamaterial with periodic blocks were limited [6]. Actually, metamaterial is not a 'true' material but a structure [7]. Composite is highly utilized and investigated due to its functionality [8–10], designability [11–14], flexibility [15–17] and easy processing [18,19]. With the requirement of turning metamaterial into a truly structural and functional integrated material, it is of significance to put up with a metacomposites whose periodic units are formed during the fabrication of metacomposites and act as the reinforcement of composite as well.

Textile structure has unique advantages in tuning electromagnetic behavior of composite due to the high structural flexibility. By adjusting textile structure from three-dimensional interlocking woven to orthogonal structure, different radar absorption properties have been presented [20,21]. Wang et al. inserted a graphene-based fabric between glass fiber and carbon fiber clothes, creating an effective microwave sandwich composite at 8–18 GHz [22]. Therefore, to realize the fabrication of integrated metacomposites, weaving technique is an option to form both the metamaterial units and reinforcement synchronously. The inherent periodic interweaving of textile structure is beneficial on forming various types the metamaterial units. It has been proven that the negative electromagnetic parameters including permittivity and permeability are mainly controlled by metamaterial unit structures rather than their composition [6,23].

Ferromagnetic microwires possess unique electromagnetic performance and have been investigated by many scholars in previous studies [-][24-27]. Owing to the giant magneto-impedance (GMI) and giant stress-impedance (GSI) effects, ferromagnetic mircowires can serve as fillers, with an attempt to obtain tunable electromagnetic performance and microwave absorption [28–32]. Moreover, the difference in the geometric form of ferromagnetic microwires also changes the electromagnetic performance of composites. Qin et al. embedded parallel Co-based ferromagnetic microwires in prepregs to make metacomposites. It was found that the field adjustable properties of metacomposites were dependent on the properties and configuration of ferromagnetic microwires [33]. Lou et al. studied the microwave performance of metacomposites that were composed of orthogonal-array $Fe_{77}Si_{10}B_{10}C_3$ microwires. The metacomposites exhibited significant natural double negative feature. In addition, different distance between ferromagnetic microwires generated different transmission level [34]. Luo et al. further compared electromagnetic performances between Co-based microwires at different lengths with the orthogonal Fe-based microwires. They found that the metacomposites had a dual-frequency transmission window at 1.5–3.5 GHz and 9–17 GHz when the distance between Co-based microwires was 10 mm [35]. However, the stacking of microwires in previous works sacrificed the integration of whole structure due to the lack of connection through the thickness direction. By introducing weave method for microwires, we propose a novelty design that can retain integration and endow functionality at the same time for the metacomposites. Meanwhile, owing to the curved morphology of microwires in textile structure, the influence of curvature can be adjusted and investigated.

In this study, tunable electromagnetic response and microwave absorption behavior of metacomposites under X and Ku bands were evaluated by changing geometrical structure of ferromagnetic periodic units, such as periodic curved length, spacing between
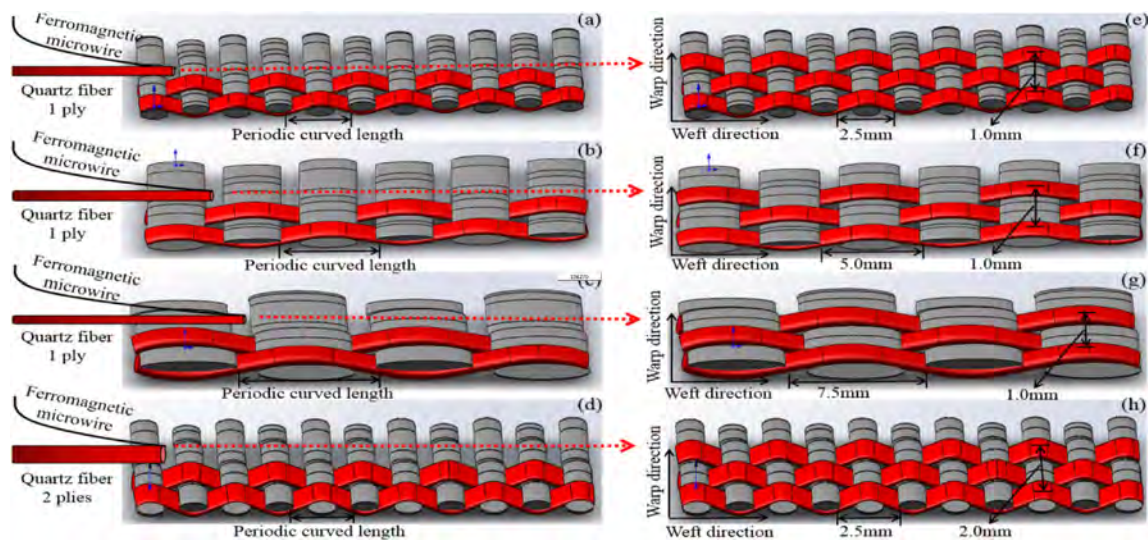

Fig. 1. Schematic diagram of textile structured preform as related to the periodic curved length being 2.5, 5, and 7.5 mm as well as spacing between ferromagnetic microwires being 0.5 and 1 mm. Red yarns represent weft yarns which locate along the width direction of fabric, and gray yarn represent warp yarns which locate along the longitudinal direction of fabric. The fine yarn is ferromagnetic microwires that are inserted with weft yarns.

Table 1
Parameters of 12 preforms of metacomposites.

| Specimen	Spacing between Microwires	Periodic Curved Length	Curvature	Arrangement Direction
S_{H1-1}	1 mm	2.5 mm	0.25	Horizontal Arrangement
S_{V1-1}				Vertical Arrangement
S_{H1-2}		5.0 mm	0.13	Horizontal Arrangement
S_{V1-2}				Vertical Arrangement
S_{H1-3}		7.5 mm	0.07	Horizontal Arrangement
S_{V1-3}				Vertical Arrangement
S_{H2-1}	0.5 mm	2.5 mm	0.25	Horizontal Arrangement
S_{V2-1}				Vertical Arrangement
S_{H2-2}		5.0 mm	0.13	Horizontal Arrangement
S_{V2-2}				Vertical Arrangement
S_{H2-3}		7.5 mm	0.07	Horizontal Arrangement
S_{V2-3}				Vertical Arrangement
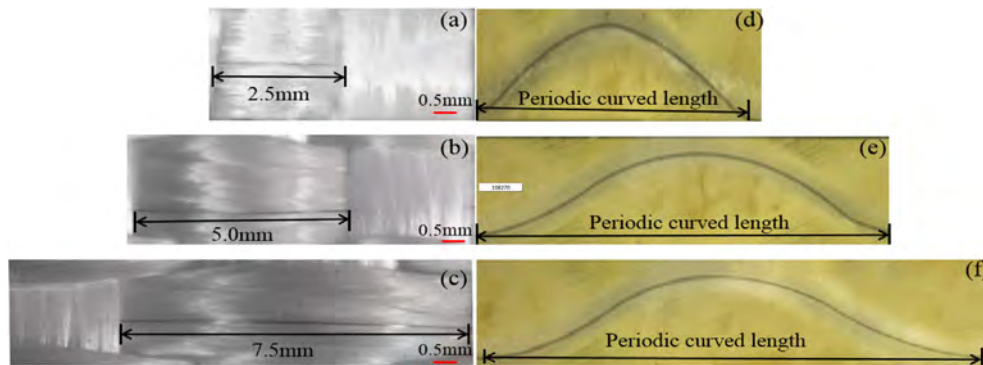
Fig. 2. Metacomposites made of periodic curved length of (a) 2.5 mm, (b) 5 mm and (c) 7.5 mm and (d−f) morphologies of corresponding cross sections.

microwires and arrangement directions. The microwave absorption mechanisms of metacomposites with absorption peaks were fully illustrated by CST simulation. The test results indicate that the employment of ferromagnetic microwires in textile structure can manipulate the electromagnetic performance and microwave absorption of metacomposites, which suggests the engineering significance in structural health monitoring, sensing and stealth applications as structure-function integrated composites
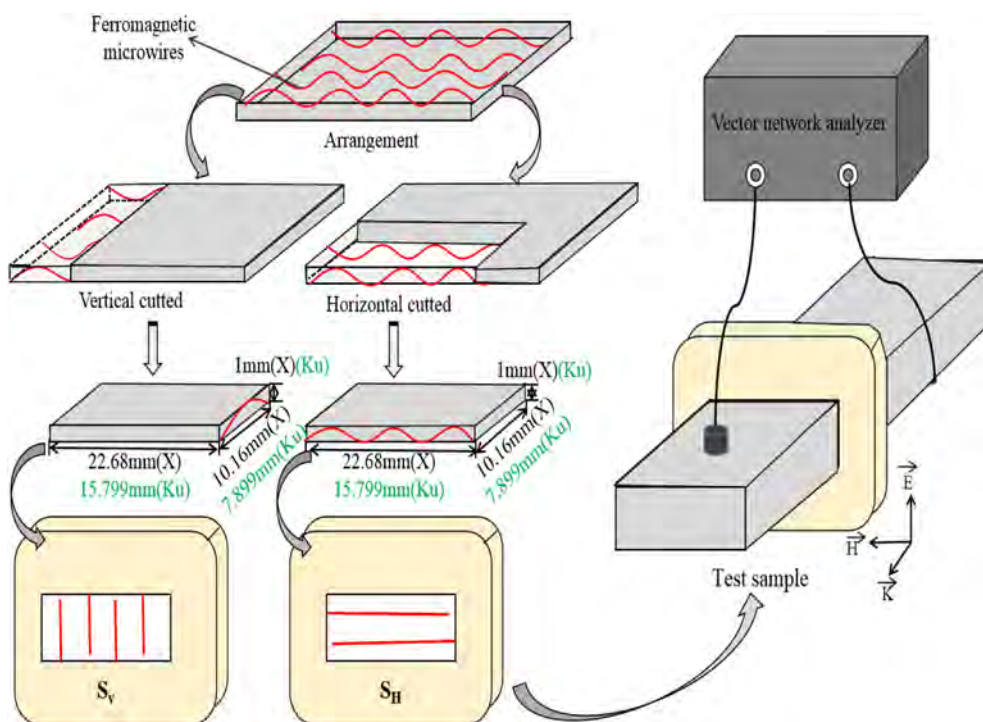

Fig. 3. Schematic diagram of horizontal and vertical arrangement of microwires in electromagnetic testing. S_H and S_V represent samples cut along the horizontal and vertical directions, respectively.

[13,36−44].

2. Experimental

2.1. Preparation of preforms containing periodic curved ferromagnetic microwires

Quartz yarns were chosen as the perform materials due to the low dielectric loss ($\tan\delta = 0.003$) and wave transmission. In the plain weave preform, warp and weft yarns were type D quartz yarns (Hubei Feilihua Quartz Glass Co., Ltd., China) with a density of 2.2 g/cm3 and a fineness of 190×4 tex. $Co_{68}Fe_4Si_{11}B_{13}Ni_1Mo_{2.3}$ ferromagnetic microwires produced by Taylor-Ulitovsky method have skin-core structure, with alloy as core and glass as skin. The outer diameter of microwire is 23 μm, and the alloy core diameter is 10.3 μm. Due to its specific alloy composition, the microwires can be spun continuously. The Co-rich element provides the microwires with excellent soft magnetic property, which is critical for electromagnetic response of metacomposite. Ferromagnetic microwires were inserted along with the weft yarns during the weaving process. Based on the Peirce geometric model of plain fabric, periodic curved lengths and curvatures of ferromagnetic microwires in different metacomposites can be calculated, shown in Fig. 1. By controlling the ply number of weft yarns, spacing between ferromagnetic microwires were adjusted to 0.5 mm and 1 mm. The detailed parameters for each specimen, including spacing between microwires, periodic curved length, microwires curvature and arrangement direction are summarized in Table 1.

2.2. Fabrication of metacomposites with textile reinforcement

Resin transfer molding (RTM) with a mold size of 380 mm × 180 mm × 1 mm was applied for fabrication; 100 ml of TDE-86 epoxy resin (Tianjin Jingdong Chemical Composite Materials Co., Ltd., China) and 27.5 ml of anhydride (Tianjin Jingdong Chemical Composite Materials Co., Ltd., China) were blended and injected into mold for curing. Fig. 2(d−f) shows the cross section of metacomposites with different periodic curved length of the ferromagnetic microwires, and the corresponding top view are presented in Fig. 2(a−c). For the electromagnetic testing, five samples for each specification were cut along the vertical or horizontal directions, respectively (Fig. 3). Sample size was 22.68 mm × 10.16 mm × 1 mm for the X-band testing and 15.799 mm × 7.899 mm × 1 mm for the Ku-band testing.

2.3. Electromagnetic characterization of textile structured metacomposites

WR-90 waveguide (22.68 mm*10.16 mm*1 mm) for X-band and rectangular WR-62 waveguide (15.799 mm*7.899 mm*1 mm) for Ku-band were used for testing. The S parameter was measured and recorded every 0.005 GHz in the X- and Ku-bands using vector network analyzer (Rohde&Schwarz ZNB 40, Rohde & Schwarz, Germany), after which S parameter was used to compute complex permittivity and permeability using the Nicolsone Rosse Weir (NRW) algorithm. Based on the transmission line theory, microwave absorption (A) were calculated by S_{11} and S_{21} [45]:

$$A = 1 − |S11|2 − |S21|2 \tag{1}$$

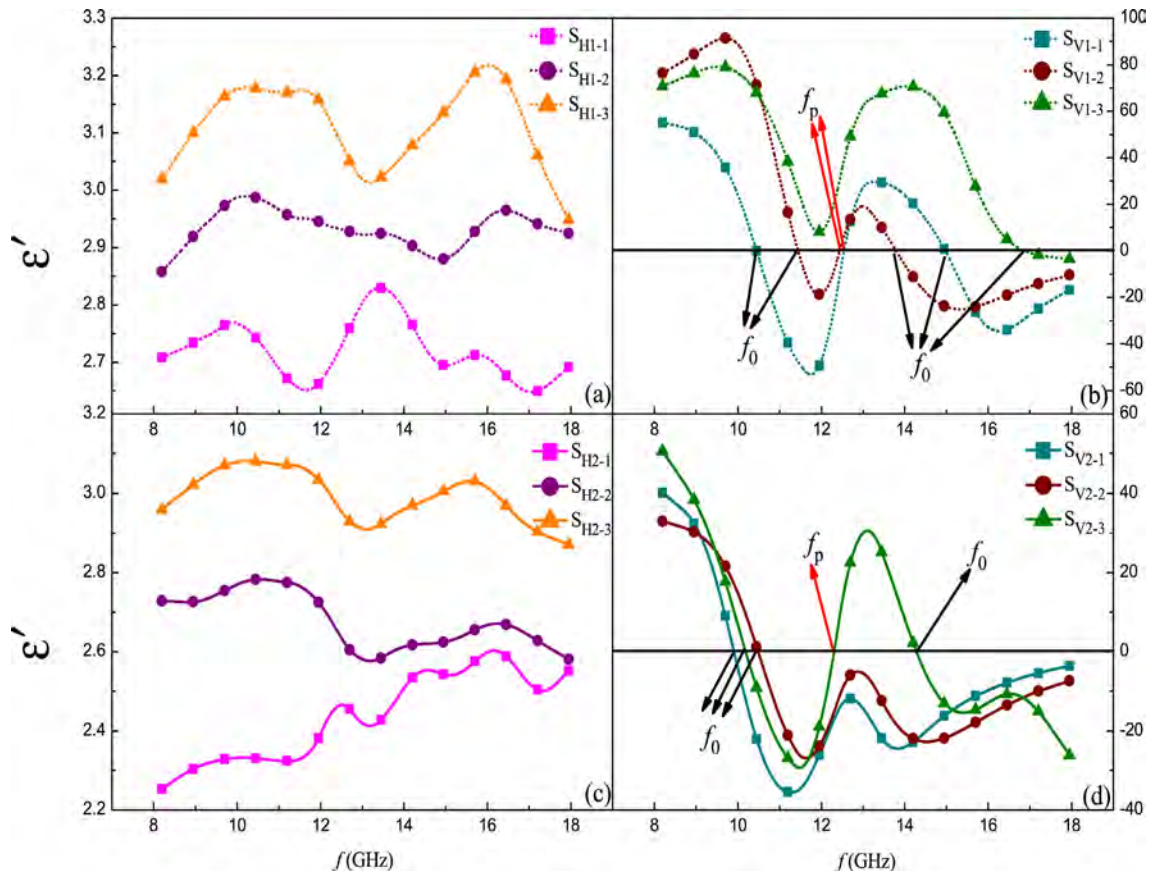CST Microwave Studio was used to simulate reflectivity, electric

Fig. 4. The real part of permittivity of metacomposites with different arrangement direction ((a) and (c) represent horizontally arranged; (b) and (d) represent vertically arranged) and microwires spacing ((a) and (b) are 1 mm; (c) and (d) are 0.5 mm) under X and Ku bands.

field distribution, magnetic field distribution and power loss of metacompoistes.

3. Results and discussion

3.1. Electromagnetic behavior of metacomposites

3.1.1. Electromagnetic response as related to periodic curved length and spacing

The real part of permittivity changing with frequency for metacomposites containing horizontally arranged microwires are shown in Fig. 4 (a) and (c). With the increase of periodic curved length from 2.5 mm to 7.5 mm, the metacomposites exhibit enhancive permittivity for both 1 mm and 0.5 mm micowires spacing. For 1 mm spacing (Fig. 4(a)), the three metacomposites exhibit characteristic peaks at a frequency of 10 GHz. However, the characteristic peaks gradually broaden as a result of increasing the periodic curved length, especially under periodic curved length of 7.5 mm, the bandwidth of characteristic peak reaches 2 GHz. The reason for this phenomenon is that with the increase of the periodic curved length of ferromagnetic microwires, the longer microwires float leads to the contact between ferromagnetic microwires, thus significantly weakening the dielectric polarizability and altering the position of polarization peaks. Moreover, S_{H1-3} demonstrates a significant characteristic peak at 15.9 GHz, which can be explicated by improved dielectricization caused by the relieved internal stress under the smallest curvature. When the spacing between ferromagnetic microwires is 0.5 mm (Fig. 4(c)), the characteristic peaks of permittivity of three metacomposites are less obvious. Especially for S_{H2-1}, when frequency rising from X-band to Ku-band, the real part of permittivity of S_{H2-1} exhibits a distinctive rise. In addition, with a specified spacing between ferromagnetic microwires being 1 mm, a shorter periodic curved

length makes stronger dependent on the frequency. But overall, the real part of permittivity of metacomposites containing horizontally arranged microwires has lower values and less dependence on frequency compared with those containing vertically arranged microwires due to the low content of ferromagnetic microwires.

The ferromagnetic microwires in the horizontally arranged metacomposites are parallel to the direction of electrical field, causing a dramatic change for the real part of the permittivity below and above zero. For metacomposites composed of a 1 mm spacing between ferromagnetic microwires (Fig. 4 (b)), S_{V1-1} and S_{V1-2} undergo natural resonances (f_0) and plasma resonances (f_p) within the X-band and their real part of permittivity reaches a negative value between f_0 and f_p, which is not observed for S_{V1-3}. It is surmised that S_{V1-3} is composed of ferromagnetic microwires with a longer periodic curved length, which is prone to deformation during RTM process and increase the microwires connectivity and then decreases the polarizability and eventually affects the dielectricization [46–51]. In addition, in the X-band, $f_0(S_{V1-1})$ is lower than $f_0(S_{V1-2})$, indicating that the resonance frequency increases as a result of a rise in the periodic curved length, proving that shorter periodic length is beneficial to broaden the operating frequency. Interestingly, all of S_{V1-1}, S_{V1-2}, and S_{V1-3} exhibit natural resonance when the frequency shifts to the Ku-band where it can be found that $f_0(S_{V1-2})<f_0(S_{V1-1})<f_0(S_{V1-3})$. Therefore, the natural resonance is correlated with both periodic curved length and curvature of ferromagnetic microwires.

Different from 1 mm spacing circumstance, all of S_{V2-1}, S_{V2-2}, and S_{V2-3} exhibit natural resonance around 10.5 GHz under X-band when the spacing between ferromagnetic microwires is decreased to 0.5 mm. This is because the number of ferromagnetic microwires in the metacomposites increases with the decrease of spacing, resulting in natural resonance of the S_{V2-3} in the X-band. Nonetheless, when it reaches to Ku-band, different
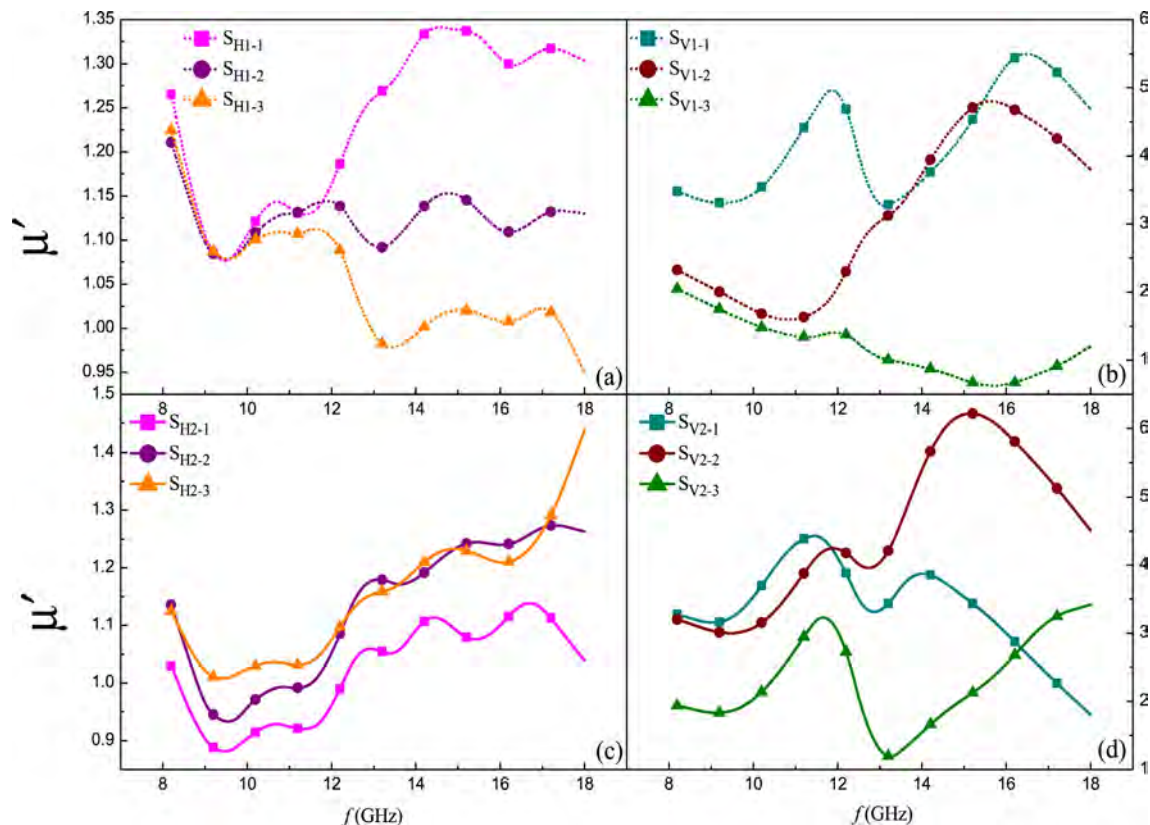

Fig. 5. The real part of permeability of metacomposites with different arrangement directions ((a) and (c) represent horizontally arranged; (b) and (d) represent vertically arranged) and microwires spacing ((a) and (b) are 1 mm; (c) and (d) are 0.5 mm) under X and Ku bands.

phenomenon comes out, that is, only S_{V2-3} exhibits plasma resonance, while the permittivity of S_{V2-1} and S_{V2-2} keep negative constantly after 10.5 GHz. According to the expression of f_p [35,52−55]:

$$f_p^2 = \frac{c^2}{2\pi b^2 \ln\left(\frac{b}{a_{eff}}\right)} \tag{2}$$

where $c = 3 \times 10^8 \text{m/s}$, b and a_{eff} denote the vacuum light velocity, microwires spacing and effective diameter. The f_p is inversely proportional to microwires spacing, therefore, f_p of S_{V2-1} and S_{V2-2} with 0.5 mm spacing is presumed to be above 12.5 GHz. Based on the tendency of Fig. 4(d), it is highly possible that the f_p appears after 18 GHz, which proves again that the shorter periodic curved length helps to reach a broadband frequency range with single-negative property.

The real part of permeability of horizontally arranged metacomposites with 1 mm spacing is presented in Fig. 5(a), and all of the three metacomposites exhibit a similar trend before 12 GHz. However, a drastic dispersion phenomenon comes up with the increasing of frequency in Ku-band. As the frequency goes up, S_{H1-1} shows an increasing permeability, S_{H1-2} does not fluctuate much, while S_{H1-3} has a decreasing permeability. Although the three metacomposites show different levels of dependence on frequency, their permeability value does not change significantly, varying from 0.95 to 1.35. When the spacing between microwires decreases to 0.5 mm, it is shown in Fig. 5(c) that the permeability of all metacomposites fluctuates and increases within a small range, which is attributed to the periodic curved alignment of microwires. In addition, for vertically arranged metacomposites with a 1 mm spacing, the permeability demonstrates double characteristic peaks for S_{V1-1}, single characteristic peak for S_{V1-2}, and zero characteristic peak for S_{V1-3} with the periodic curved length increasing from 2.5 mm to 7.5 mm (Fig. 5(b)). This phenomenon may be ascribed to two factors: curvature difference and the periodic curved length of microwires. Curvature difference formed in different textile structure triggers the rearrangement of domain structure of ferromagnetic microwires, which in turn affects the magnetization of ferromagnetic microwires. Since the micowires volume fraction is constant in three metacomposites, the S_{V1-1} containing 2.5 mm periodic curved length contains the most polarized dipoles, thus having the strongest dynamic response when interacting with electromagnetic waves [46]. When the spacing between ferromagnetic microwires decreases to 0.5 mm, the permeability of metacomposites is highly dependent on the frequency, exemplified by double characteristic peaks of both S_{V2-1} and S_{V2-2} and single characteristic peak of S_{V2-3} in X-band (Fig. 5(d)). Similarly, shorted periodic curved length intensifies the dynamics response towards electromagnetic waves. Meanwhile, a smaller spacing enhances the
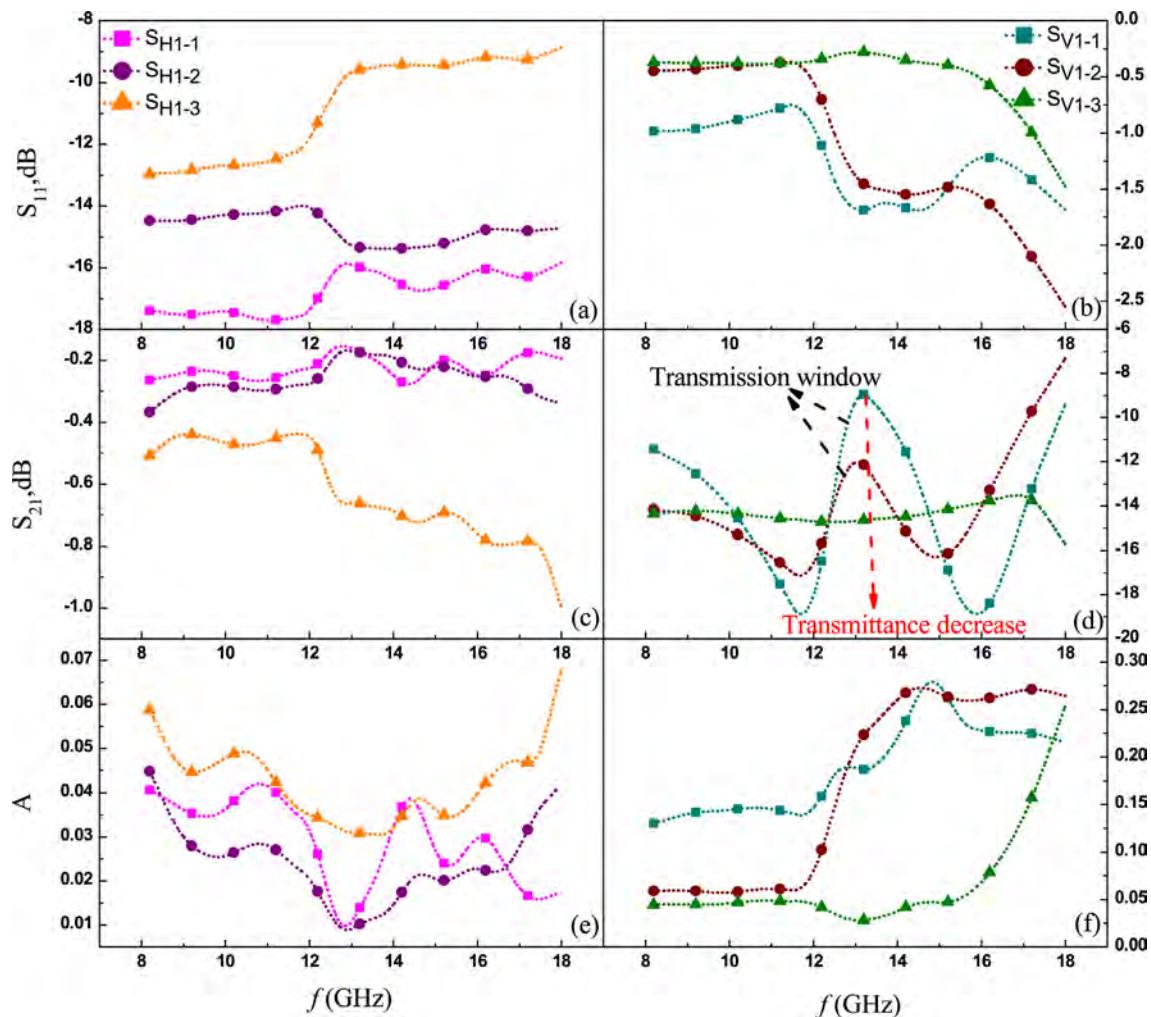

Fig. 6. The reflection (S_{11}), transmission (S_{21}), and absorption (A) of horizontally arranged (a,c,e) and vertically arranged (b,d,f) metacomposites as related to the periodic curved length of 2.5, 5, and 7.5 mm. The specified spacing between ferromagnetic microwires is 1 mm.

magnetic energy storage capacity of metacomposites.

3.1.2. Reflection, transmission and absorption as related to periodic curved length and spacing

Through Fig. 6, it can be observed that the electromagnetic propagation mechanisms for horizontally and vertically arranged metacomposites are quite different. For horizontal arranged metacomposites composed of 1 mm spacing between microwires, Fig. 6(c) indicates that the microwave transmission level is considerably high and over 90% while the microwave reflection and absorption levels are both low. This is due to the low impedance matching of horizontally arranged metacomposites, and the electromagnetic waves just directly penetrate the composite without entering the interior. This result is in conformity with the lower values of permittivity and permeability of horizontally arranged metacomposites (Figs. 4(a) and Fig. 5 (a)). The real part of permittivity and permeability represents the storage capacity of electrical and magnetic energy. With a low storage capacity, the microwave absorption of horizontally arranged metacomposites is consequently low, which is only approximately 7%.

For vertically arranged metacomposites, the microwave transmission has been mitigated, and the absorption level is improved considerably. Specifically, S_{V1-1} has the optimal microwave

absorption of 27%, which is four times greater than that of horizontally arranged counterpart. Fig. 6 (d) shows that around 13 GHz, both S_{V1-1} and S_{V1-2} display significant transmission windows which are caused by the negative permittivity occurring at plasma frequency. In addition, the frequency range of transmission window is consistent with those of permittivity characteristic peak. By contrast, S_{V1-3} does not display negative permittivity and transmission window is thus absent. An increase in periodic curved length from 2.5 mm to 5 mm adversely affects the breadth of transmission, and the window disappears as a result of a periodic curved length being 7.5 mm, which suggests that with a 1 mm spacing between microwires, periodic curved length dominates the presence of transmission window.

In the absorption spectrum, the absorption peak of S_{V1-1} occurs at 15 GHz because of the presence of natural resonance at this specified frequency as in Fig. 4 (b). Moreover, S_{V1-1} and S_{V1-2} are also sensitive to the frequency where the microwave absorption has an instant rise as a result of the presence of transmission window. S_{V1-3} demonstrates a quick rise in the microwave absorption when the frequency is higher than 17 GHz, which is ascribed to the natural resonance and a faint transmission window at this specified frequency. Therefore, transmission window caused by negative permittivity can strengthen the absorption ability of
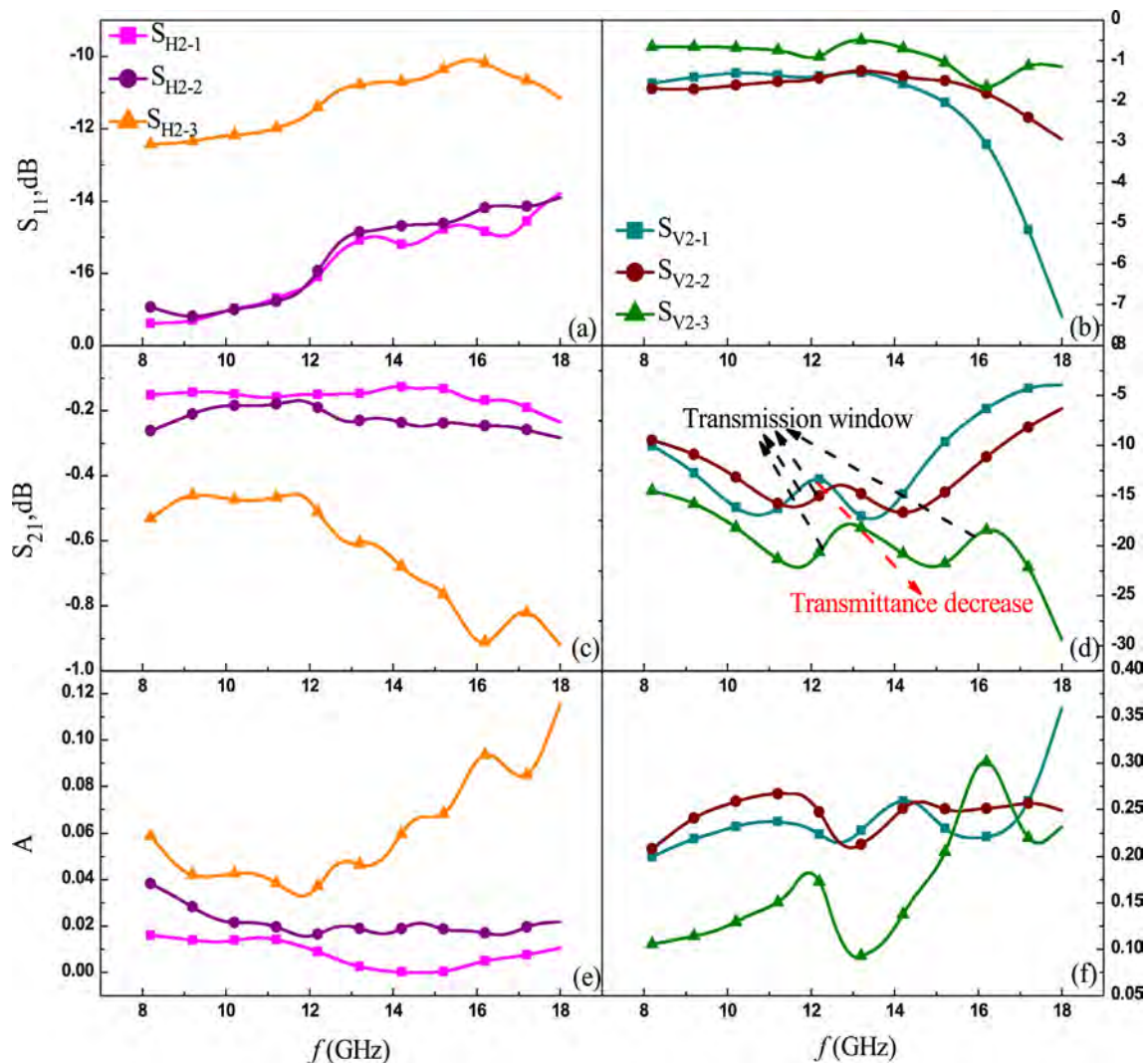

Fig. 7. The reflection (S_{11}), transmission (S_{21}), and absorption (A) of horizontally arranged (a,c,e) and vertically arranged (b,d,f) metacomposites as related to the periodic curved length of 2.5, 5, and 7.5 mm. The specified spacing between ferromagnetic microwires is 0.5 mm.
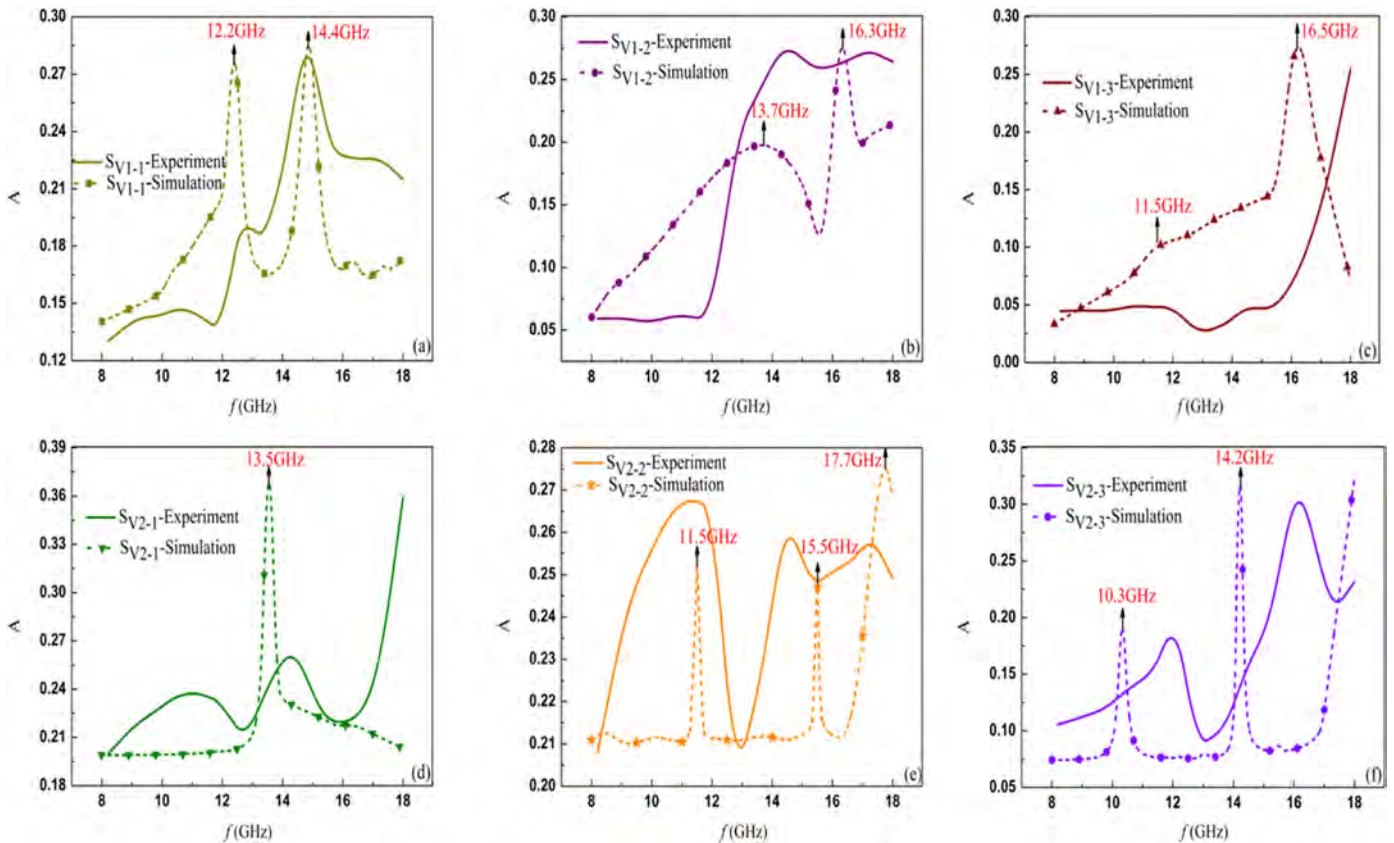
Fig. 8. Experimental and simulation comparison of absorption spectrums of vertically arranged metacomposites.

metacomposites.

Regardless of whether the spacing between microwires being 1 mm or 0.5 mm, horizontally arranged metacomposites have a higher microwave transmission level, which is equivalently low microwave absorption. However, S_{H2-3} has a significantly greater microwave absorption in Ku-band where S_{H2-3} exhibits a more significant dielectric polarization peak of the permittivity than S_{H2-1} and S_{H2-2}. For vertically arranged metacomposites, with the decrease of spacing, both reflection and transmission decrease, thus resulting in increased absorption. In the transmission spectrum (Fig. 7(d)), double transmission windows appear for sample with 7.5 mm periodic curved length, which corresponds to the double characteristic peaks of permittivity. Blue-shift of transmission window can be observed with the increasing of the periodic curved length. In the absorption spectrum, S_{V2-3} exhibits double absorption peaks, one is caused by plasma resonance around 12 GHz and the other is caused by the natural ferromagnetic resonance at 16.2 GHz. Although S_{V2-3} exhibits double absorption peaks, the optimal microwave absorption of 36% occurs when the periodic curved length is 2.5 mm. In sum, a decrease in the spacing between ferromagnetic microwires from 1 mm to 0.5 mm has a positive influence on the absorption level.

3.2. Electromagnetic wave absorption mechanism

3.2.1. Simulation and experimental comparison of electromagnetic wave absorption characteristics

In order to validate the design of textile based metacomposites and further elaborate the electromagnetic response mechanism, CST Microwave Studio® was used to simulate the three-dimensional electromagnetic absorption characteristics. The simulations were only conducted for vertically arranged

metacomposistes since the electromagnetic response and single-negative property are remarkable in vertical arrangement. According to comparisons between the simulation and experimental results in Fig. 8, peak shifts and value differences exist between the simulation and the experimental results, probably resulting from fabrication error and quartz yarn coverage. Shown in Fig. 2, ferromagnetic microwires are periodically covered by insulating quartz yarns, causing the inconsistency of dielectric and magnetic responses. For the overall trend, qualitative analysis can be done on absorption peaks where absorption resonances take place most intensively in these frequency points [56]. The absorption peaks in Fig. 8(a)–(f) locate at 12.2 GHz and 14.4 GHz for S_{V1-1}, 13.7 GHz and 16.3 GHz for S_{V1-2}, 11.5 GHz and 16.5 GHz for S_{V1-3}, 13.5 GHz for S_{V2-1}, 11.5 GHz, 15.5 GHz and 17.7 GHz for S_{V2-2}, and 10.3 GHz and 14.2 GHz for S_{V2-3}, respectively. The period-average amplitude of electric field intensity, magnetic field intensity and power loss distribution are simulated and investigated in the following sections.

3.2.2. Effects of periodic curved length on electromagnetic wave absorption mechanism

From the power loss distribution in Fig. 9, it can be observed clearly that with the increase of periodic curved length, the intensity and distribution gradually fade away, which is consistent with experimental results in Fig. 6(f). Although the power loss is a combination of electric loss and magnetic loss, the major distribution areas of electric field and power loss overlap each other, indicating that the major loss for the textile structured metacomposites under X and Ku bands derives from electric loss, which is consistent with Huang et al.'s work [56].

For metacomposites with periodic curved length of 2.5 mm, under 12.2 GHz, the electric field concentrates on the edge of
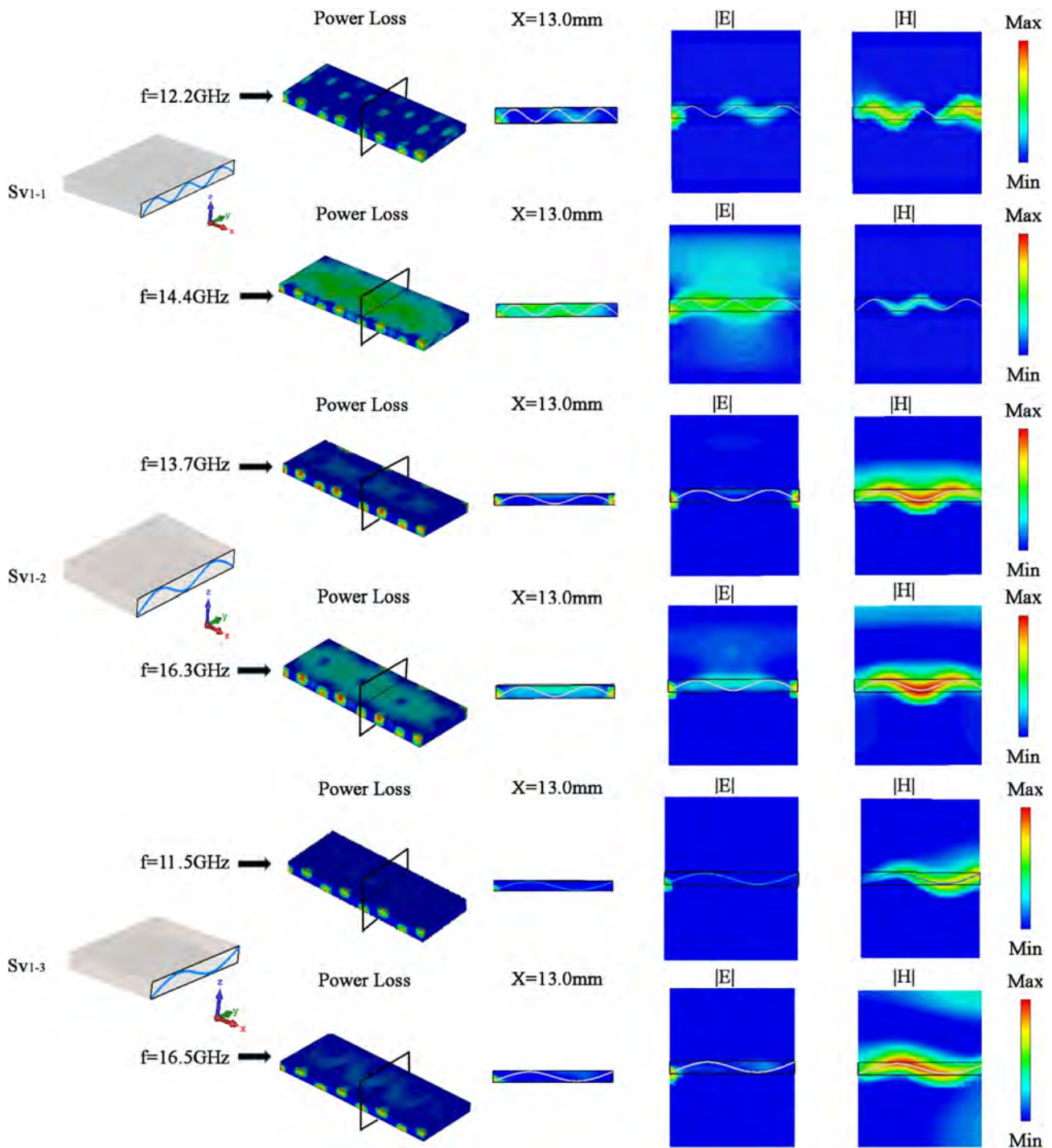
Fig. 9. The complex electric field intensity time-average amplitude distribution, complex magnetic field intensity time-average amplitude distribution and power loss distribution of vertically arranged meacomposites with periodic length of 2.5 mm, 5 mm, 7.5 mm in different absorption peaks respectively.

composite, while magnetic field is prisoned inside the ferromagnetic mircowires. At 14.4 GHz, the oval electric field appears and leads to the large area distribution on composite. Similar oval electric field can be seen for S_{V1-2} at 16.3 GHz, but the intensity is weakened. The magnetic field is still distributed following the pattern of microwires interweaving. Therefore, the power loss is correspondingly decreased. For S_{V1-3} with longest periodic curved length being 7.5 mm, the distribution of magnetic field continues to follow the path of microwires, however, the electric field only concentrates on the left edge of composite, showing a relenting

intensity with the increase of periodic curved length. In addition, the distribution pattern of power loss directly reflect the varied periodic curved length, that is, small periodic curved length in S_{V1-1} tend to form uniform distribution, while larger one is prone to generate spread pattern with minimum loss occurring at the curvature points. This explains why metacomposites with small periodic curved length has stronger electromagnetic response and higher microwave absorption. Compared with the two frequency points of absorption peaks for each metacomposites, higher frequency causes more severe power loss, probably because
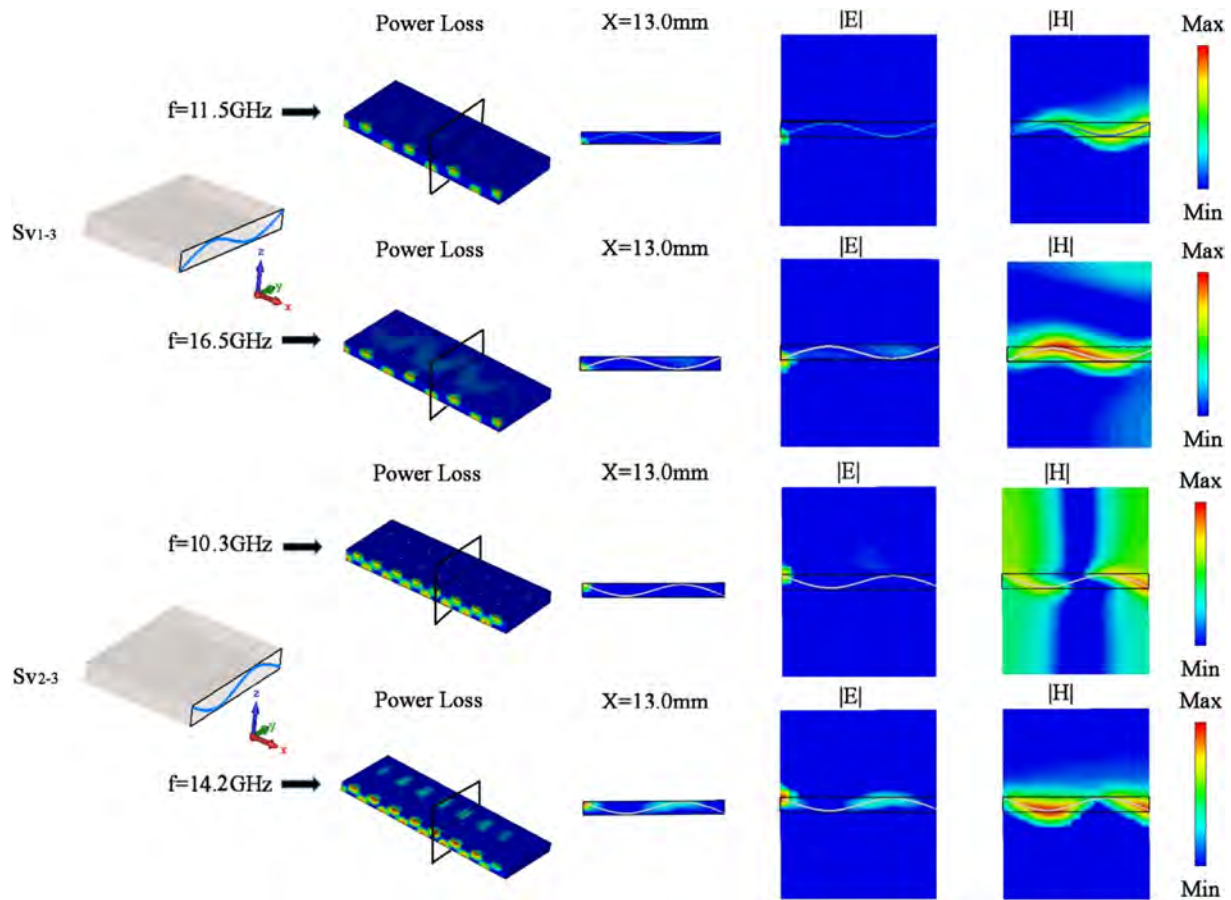
Fig. 10. The complex electric field intensity time-average amplitude distribution, complex magnetic field intensity time-average amplitude distribution and power loss distribution of vertically arranged meacomposites with spacing of 1 mm, 0.5 mm in different absorption peaks respectively.

permittivity turns negative after 14 GHz and contributes to the dielectric loss, shown in Fig. 4(b).

3.2.3. Effects of microwires spacing on electromagnetic wave absorption mechanism

The microwave absorption simulation on S_{V1-3} and S_{V2-3} are presented in Fig. 10 in terms of complex electric field intensity time-average amplitude distribution, complex magnetic field intensity time-average amplitude distribution and power loss distribution. Compared with the periodic curved length effect, the change of spacing does not aggravate power loss by much, although magnetic field distorts when microwires spacing is reduced to 0.5 mm, possibly caused by the double increase of microwires. Electric field concentrates on the edge of composite, and with the decrease of spacing, it expands along the microwires to the middle of composite, which can be explained by the strong dynamic wire-wire interactions with microwave and giving rise to strong long range dipolar resonance (LRDR) [35]. Besides, from the power loss distribution, the donut pattern at 1 mm spacing shrinks to light spot at 0.5 mm on the composite surface, indicating that ratio of magnetic loss has been enlarged as a result of increased number of microwires, which is consistent with Fig. 5(d). When electromagnetic wave triggers magnetic domain wall motion, the magnetic domain structure vary when magnetic field H passes through the composite, which composes parts of the magnetic loss [56].

In sum, the simulation results qualitatively demonstrate the microwave propagation and absorption mechanism and support the experimental phenomenon. Further model optimization should be done in order to obtain more consistent results with

experiments.

4. Conclusion

A systematic study on the microwave properties of textile structured metacomposites containing ferromagnetic microwires with different arrangement direction, periodic curved length and microwires spacing has been conducted. The employment of textile structure realizes a geometric form of metamaterial units with tunable electromagnetic performances. The electromagnetic test results show that the vertical arrangement metacomposites exhibit negative permittivity in the X and Ku frequency ranges. When the spacing between ferromagnetic microwires decreased from 1 mm to 0.5 mm, a periodic curved length being 2.5 mm or 5 mm changes the double natural resonance to single natural resonance, but a periodic curved length being 7.5 mm goes the other way around. Composed of 0.5 mm microwires spacing and 7.5 mm periodic curved length, the metacomposites have double transmission windows corresponding to the double characteristic peaks of permittivity. Moreover, the microwave absorption of metacomposites is considerably improved by an increase in the microwires spacing, and is 27% for 1 mm and 36% for 0.5 mm. To sum up, changing the textile structure effectively changes the electromagnetic response and microwave propagation of metacomposites. In addition, through the CST simulation, the simulation results show that the major loss for the textile structured metacomposites under X and Ku bands derives from electric loss. Small periodic curved length tends to form uniform distribution, while larger one is prone to generate spread pattern with minimum loss occurring at the

curvature points. The reduction of microwires spacing induces strong long range dipolar resonance and magnetic domain wall motion, thusing improving the microwave absorption. The simulation results fully demonstrate the microwave absorption mechanism of the metacomposites with microwave absorption peak. Therefore, the metacomposites composed of a textile structure have a great potential in structural health monitoring, sensing and stealth applications as structure-function integrated composite.

CRediT authorship contribution statement

Qian Jiang: Conceptualization, Formal analysis, Writing - review & editing. **Chunjie Xiang:** Investigation, Writing - original draft, Software. **Yang Luo:** Data curation, Methodology. **Liwei Wu:** Investigation, Validation. **Qian Zhang:** Methodology, Software. **Shilu Zhao:** Methodology. **Faxiang Qin:** Resources, Supervision. **Jia-Horng Lin:** Project administration, Supervision.

Acknowledgements

References

[1] D.R. Smith, J.B. Pendry, M.C.K. Wiltshire, Metamaterials and negative refractive index, Science 305 (5685) (2004) 788–792.
[2] D. Makhnovskiy, V. Zamorovskii, J. Summerscales, Embedded ferromagnetic microwires for monitoring tensile stress in polymeric materials, Compos. Part A-Appl. S. 61 (2014) 216–223.
[3] L. Zhu, K. Li, Y. Luo, D. Yu, Z. Wang, G. Wu, J. Xie, Z. Tang, Magnetostrictive properties and detection efficiency of TbDyFe/FeCo composite materials for nondestructive testing, J. Rare Earths (**37**(2),2019,166-170).
[4] J. Valentine, S. Zhang, T. Zentgraf, E. Ulin-Avila, D.A. Genov, G. Bartal, X. Zhang, Three-dimensional optical metamaterial with a negative refractive index, Nature 455 (7211) (2008). 376–U32.
[5] J.B. Pendry, Negative refraction makes a perfect lens, Phys. Rev. Lett. 85 (18) (2000) 3966–3969.
[6] K. Sun, P. Xie, Z. Wang, T. Su, Q. Shao, J. Ryu, X. Zhang, J. Guo, A. Shankar, J. Li, R. Fan, D. Cao, Z. Guo, Flexible polydimethylsiloxane/multi-walled carbon nanotubes membranous metacomposites with negative permittivity, Polymer 125 (2017) 50–57.
[7] D. Estevez, F. Qin, Y. Luo, L. Quan, Y.-W. Mai, L. Panina, H.-X. Peng, Tunable negative permittivity in nano-carbon coated magnetic microwire polymer metacomposites, Compos. Sci. Technol. 171 (2019) 206–217.
[8] Y. Qian, Y. Yuan, H. Wang, H. Liu, J. Zhang, S. Shi, Z. Guo, N. Wang, Highly efficient uranium adsorption by salicylaldoxime/polydopamine graphene oxide nanocomposites, J. Mater. Chem. A. 6 (48) (2018) 24676–24685.
[9] H. Gu, X. Xu, J. Cai, S. Wei, H. Wei, H. Liu, D.P. Young, Q. Shao, S. Wu, T. Ding, Z. Guo, Controllable organic magnetoresistance in polyaniline coated poly(p-phenylene-2,6-benzobisoxazole) short fibers, Chem. Commun. 55 (68) (2019) 10068–10071.
[10] Y. Guo, K. Ruan, X. Yang, T. Ma, J. Kong, N. Wu, J. Zhang, J. Gu, Z. Guo, Constructing fully carbon-based fillers with a hierarchical structure to fabricate highly thermally conductive polyimide nanocomposites, J. Mater. Chem. C. 7 (23) (2019) 7035–7044.
[11] Y. Guo, X. Yang, K. Ruan, J. Kong, M. Dong, J. Zhang, J. Gu, Z. Guo, Reduced graphene oxide heterostructured silver nanoparticles significantly enhanced thermal conductivities in hot-pressed electrospun polyimide nanocomposites, ACS Appl. Mater. Interfaces 11 (28) (2019) 25465–25473.
[12] Y. He, Q. Chen, H. Liu, L. Zhang, D. Wu, C. Lu, W. OuYang, D. Jiang, M. Wu, J. Zhang, Y. Li, J. Fan, C. Liu, Z. Guo, Friction and wear of MoO3/graphene oxide modified glass fiber reinforced epoxy nanocomposites, Macromol. Mater. Eng. 304 (8) (2019).
[13] D. Jiang, Y. Wang, B. Li, C. Sun, Z. Wu, H. Yan, L. Xing, S. Qi, Y. Li, H. Liu, W. Xie, X. Wang, T. Ding, Z. Guo, Flexible sandwich structural strain sensor based on silver nanowires decorated with self-healing substrate, Macromol. Mater. Eng. 304 (7) (2019).
[14] Y. Li, T. Zhang, B. Jiang, L. Zhao, H. Liu, J. Zhang, J. Fan, Z. Guo, Y. Huang, Interfacially reinforced carbon fiber silicone resin via constructing functional nano-structural silver, Compos. Sci. Technol. 181 (2019).
[15] R. Ma, Y. Wang, H. Qi, C. Shi, G. Wei, L. Xiao, Z. Huang, S. Liu, H. Yu, C. Teng, H. Li, V. Murugadoss, J. Zhang, Y. Wang, Z. Guo, Nanocomposite sponges of sodium alginate/graphene oxide/polyvinyl alcohol as potential wound dressing: in vitro and in vivo evaluation, Compos. Part B. 167 (2019) 396–405.
[16] Y. Ma, C. Hou, H. Zhang, Q. Zhang, H. Liu, S. Wu, Z. Guo, Three-dimensional core-shell Fe3O4/Polyaniline coaxial heterogeneous nanonets: preparation and high performance supercapacitor electrodes, Electrochim. Acta 315 (2019) 114–123.
[17] G. Zhu, X. Cui, Y. Zhang, S. Chen, M. Dong, H. Liu, Q. Shao, T. Ding, S. Wu, Z. Guo, Poly (vinyl butyral)/Graphene oxide/poly (methylhydrosiloxane) nanocomposite coating for improved aluminum alloy anticorrosion, Polymer 172 (2019) 415–422.
[18] L.C. Ma, Y.Y. Zhu, P.F. Feng, G.J. Song, Y.D. Huang, H. Liu, J.X. Zhang, J.C. Fan, H. Hou, Z.H. Gou, Reinforcing carbon fiber epoxy composites with triazine derivatives functionalized graphene oxide modified sizing agent, Compos. Part B. 176 (2019) 107078.
[19] Z.Z. Zhang, J.X. Zhang, S.Y. Li, J.P. Liu, M.Y. Dong, Y.C. Li, N. Lu, S.Y. Lei, J.J. Tang, J.C. Fan, Z.H. Guo, Effect of graphene liquid crystal on dielectric properties of polydimethylsiloxane nanocomposites, Compos. Part B. 176 (2019) 107338.
[20] W. Fan, D.D. Li, J.L. Li, J.Z. Li, L.J. Yuan, L.L. Xue, R.J. Sun, J.G. Meng, Electromagnetic properties of three-dimensional woven carbon fiber fabric/epoxy composite, Text. Res. J. 88 (20) (2018) 2353–2361.
[21] W. Fan, L.J. Yuan, N. D'Souza, B.G. Xu, W.S. Dang, L.L. Xue, J.Z. Li, C. Tonoy, R.J. Sun, Enhanced mechanical and radar absorbing properties of carbon/glass fiber hybrid composites with unique 3D orthogonal structure, Polym. Test. 69 (2018) 71–79.
[22] X.X. Wang, C.M. Sun, F.B. Wen, S.Y. Jiang, M.S. Cao, Strong mechanics and broadened microwave absorption of graphene-based sandwich structures and surface-patterned structures, J. Mater. Sci. Mater. Electron. 29 (11) (2018) 9683–9691.
[23] M. Chen, X. Wang, Z. Zhang, K. Sun, C. Cheng, F. Dang, Negative permittivity behavior and magnetic properties of C/YIG composites at radio frequency, Mater. Des. 97 (2016) 454–458.
[24] D.P. Makhnovskiy, L.V. Panina, C. Garcia, A.P. Zhukov, J. Gonzalez, Experimental demonstration of tunable scattering spectra at microwave frequencies in composite media containing CoFeCrSiB glass-coated amorphous ferromagnetic wires and comparison with theory, Phys. Rev. B. 74 (6) (2006).
[25] A.V. Ivanov, A.N. Shalygin, V.Y. Galkin, A.V. Vedyayev, V.A. Ivanov, Meta-materials from amorphous ferromagnetic microwires: interaction between microwires, in: N. Perov (Ed.), J. Magn. Magn. Mater., 2009, 357–+.
[26] Y. Luo, H.X. Peng, F.X. Qin, M. Ipatov, V. Zhukova, A. Zhukov, J. Gonzalez, Fe-based ferromagnetic microwires enabled meta-composites, Appl. Phys. Lett. 103 (25) (2013).
[27] F.X. Qin, H.X. Peng, Z. Chen, H. Wang, J.W. Zhang, G. Hilton, Optimization of microwire/glass-fibre reinforced polymer composites for wind turbine application, Appl. Phys. Mater. Sci. Process 113 (3) (2013) 537–542.
[28] F. Qin, H.-X. Peng, Ferromagnetic microwires enabled multifunctional composite materials, Prog. Mater. Sci. 58 (2) (2013) 183–259.
[29] O. Reynet, A.L. Adenot, S. Deprot, O. Acher, M. Latrach, Effect of the magnetic properties of the inclusions on the high-frequency dielectric response of diluted composites, Phys. Rev. B. 66 (9) (2002).
[30] D.P. Makhnovskiy, L.V. Panina, Field dependent permittivity of composite materials containing ferromagnetic wires, J. Appl. Phys. 93 (7) (2003) 4120–4129.
[31] F. Qin, V.V. Popov, H.-X. Peng, Stress tunable microwave absorption of ferromagnetic microwires for sensing applications, J. Alloy. Comp. 509 (39) (2011) 9508–9512.
[32] F.X. Qin, H.X. Peng, V.V. Popov, L.V. Panina, M. Ipatov, V. Zhukova, A. Zhukov, J. Gonzalez, Stress tunable properties of ferromagnetic microwires and their multifunctional composites, J. Appl. Phys. 109 (7) (2011).
[33] F.X. Qin, H.X. Peng, M.H. Phan, L.V. Panina, M. Ipatov, A. Zhukov, Effects of wire properties on the field–tunable behaviour of continuous-microwire composites, Sens. Actuator A-Phys. 178 (2012) 118–125.
[34] Y. Luo, H.X. Peng, F.X. Qin, M. Ipatov, V. Zhukova, A. Zhukov, J. Gonzalez, Metacomposite characteristics and their influential factors of polymer composites containing orthogonal ferromagnetic microwire arrays, J. Appl. Phys. 115 (17) (2014).
[35] Y. Luo, F.X. Qin, F. Scarpa, J. Carbonell, M. Ipatov, V. Zhukova, A. Zhukov, J. Gonzalez, L.V. Panina, H.X. Peng, Microwires enabled metacomposites towards microwave applications, J. Magn. Magn. Mater. 416 (2016) 299–308.
[36] H. Liu, Q. Li, S. Zhang, R. Yin, X. Liu, Y. He, K. Dai, C. Shan, J. Guo, C. Liu, C. Shen, X. Wang, N. Wang, Z. Wang, R. Wei, Z. Guo, Electrically conductive polymer composites for smart flexible strain sensors: a critical review, J. Mater. Chem. C. 6 (45) (2018) 12121–12141.
[37] C. Wang, V. Murugadoss, J. Kong, Z. He, X. Mai, Q. Shao, Y. Chen, L. Guo, C. Liu, S. Angaiah, Z. Guo, Overview of carbon nanostructures and nanocomposites for electromagnetic wave shielding, Carbon 140 (2018) 696–733.
[38] H. Wei, H. Wang, Y. Xia, D. Cui, Y. Shi, M. Dong, C. Liu, T. Ding, J. Zhang, Y. Ma, N. Wang, Z. Wang, Y. Sun, R. Wei, Z. Guo, An overview of lead-free piezoelectric materials and devices, J. Mater. Chem. C. 6 (46) (2018) 12446–12467.
[39] P. Xie, H. Li, B. He, F. Zhang, J. Lin, R. Fan, C. Hou, H. Liu, J. Zhang, Y. Ma, Z. Guo, Bio- gel derived nickel/carbon nanocomposites with enhanced microwave absorption, J. Mater. Chem. C. 6 (32) (2018) 8812–8822.
[40] H. Gu, H. Zhang, C. Ma, H. Sun, C. Liu, K. Dai, J. Zhang, R. Wei, T. Ding, Z. Guo, Smart strain sensing organic- inorganic hybrid hydrogels with nano barium ferrite as the cross- linker, J. Mater. Chem. C. 7 (8) (2019) 2353–2360.

[41] Q. Li, H. Liu, S. Zhang, D. Zhang, X. Liu, Y. He, L. Mi, J. Zhang, C. Liu, C. Shen, Z. Guo, Superhydrophobic electrically conductive paper for ultrasensitive strain sensor with excellent anticorrosion and self-cleaning property, ACS Appl. Mater. Interfaces 11 (24) (2019) 21904–21914.

[42] T. Liang, L. Qi, Z. Ma, Z. Xiao, Y. Wang, H. Liu, J. Zhang, Z. Guo, C. Liu, W. Xie, T. Ding, N. Lu, Experimental study on thermal expansion coefficient of composite multi-layered flaky gun propellants, Compos. Part B. 166 (2019) 428–435.

[43] N. Wu, D. Xu, Z. Wang, F. Wang, J. Liu, W. Liu, Q. Shao, H. Liu, Q. Gao, Z. Guo, Achieving superior electromagnetic wave absorbers through the novel metal-organic frameworks derived magnetic porous carbon nanorods, Carbon 145 (2019) 433–444.

[44] D. Jiang, V. Murugadoss, Y. Wang, J. Lin, T. Ding, Z. Wang, Q. Shao, C. Wang, H. Liu, N. Lu, R. Wei, A. Subramania, Z. Guo, Electromagnetic interference shielding polymers and nanocomposites-A review, Polym. Rev. 59 (2) (2019) 280–337.

[45] D.K. Ghodgaonkar, V.V. Varadan, V.K. Varadan, A free-space method for measurement of dielectric constants and loss tangents at microwave frequencies, IEEE Trans. Instrum. Meas. 38 (3) (1989) 789–793.

[46] Y. Luo, H.X. Peng, F.X. Qin, B.J.P. Adohi, C. Brosseau, Magnetic field and mechanical stress tunable microwave properties of composites containing Fe-based microwires, Appl. Phys. Lett. 104 (12) (2014) 121912.

[47] P. Xie, Z. Wang, Z. Zhang, R. Fan, C. Cheng, H. Liu, Y. Liu, T. Li, C. Yan, N. Wang, Z. Guo, Silica microsphere templated self-assembly of a three-dimensional carbon network with stable radio-frequency negative permittivity and low dielectric loss, J. Mater. Chem. C 6 (19) (2018) 5239–5249.

[48] C. Cheng, R. Fan, G. Fan, H. Liu, J. Zhang, J. Shen, Q. Ma, R. Wei, Z. Guo, Tunable negative permittivity and magnetic performance of yttrium iron garnet/polypyrrole metacomposites at the RF frequency, J. Mater. Chem. C. 7 (11) (2019) 3160–3167.

[49] H. Gu, X. Xu, M. Dong, P. Xie, Q. Shao, R. Fan, C. Liu, S. Wu, R. Wei, Z. Guo, Carbon nanospheres induced high negative permittivity in nanosilver-polydopamine metacomposites, Carbon 147 (2019) 550–558.

[50] K. Sun, J. Xin, Z. Wang, S. Feng, Z. Wang, R. Fan, H. Liu, Z. Guo, Weakly negative permittivity and low frequency dispersive behavior in graphene/epoxy metacomposites, J. Mater. Sci. Electron. 30 (15) (2019) 14745–14754.

[51] K. Sun, R. Fan, X. Zhang, Z. Zhang, Z. Shi, N. Wang, P. Xie, Z. Wang, G. Fan, H. Liu, C. Liu, T. Li, C. Yan, Z. Guo, An overview of metamaterials and their achievements in wireless power transfer, J. Mater. Chem. C. 6 (12) (2018) 2925–2943.

[52] K. Sun, J.H. Xin, Y.P. Li, Z.Y. Wang, Q. Hou, X.F. Li, X.F. Wu, R.H. Fan, K.L. Choy, Negative permittivity derived from inductive characteristic in the percolating Cu/EP metacomposites, J. Mater. Sci. Technol. 35 (2019) 2463.

[53] H. Wu, X. Huang, L. Qian, Preparation, mechanism and property of metacomposites with carbon materials as fillers, Eng. Sci. 2 (2018) 17–25.

[54] K. Sun, J.N. Dong, Z.X. Wang, Z.Y. Wang, G.H. Fan, Q. Hou, L.Q. An, M.Y. Dong, R.H. Fan, Z.H. Guo, Tunable negative permittivity in flexible graphene/PDMS metacomposites, J. Phys. Chem. C 123 (2019) 23635.

[55] H.K. Wu, Y. Zhang, R. Yin, W. Zhao, X.M. Li, L. Qian, Magnetic negative permittivity with dielectric resonance in random Fe_3O_4@graphene-phenolic resin composites, Adv. Compos. Hybrid Mater. 1 (2018) 68–176.

[56] Y. Huang, W.-L. Song, C. Wang, Y. Xu, W. Wei, M. Chen, L. Tang, D. Fang, Multi-scale design of electromagnetic composite metamaterials for broadband microwave absorption, Compos. Sci. Technol. 162 (2018) 206–214.